JOURNAL OF PROPULSION AND POWER
Vol. 26, No. 4, July–August 2010

Swirling Airflow Through a Nozzle: Choking Criteria

A. Abdelhafez* and A. K. Gupta†
University of Maryland, College Park, Maryland 20742

DOI: 10.2514/1.47956

The choking criteria, thrust, and specific impulse of swirling airflow through a choked nozzle are investigated both numerically and experimentally. The effects of swirl are examined at matched nozzle reservoir pressure as well as matched mass flow. A convergent nozzle is used to generate the underexpanded airflow. It was found that the throat velocity itself (and not any of its components) is choked in a swirling flowfield. Therefore, the limiting tangential Mach number is unity, and the application of swirl always results in a reduction in the axial Mach number component. The velocity is choked all over the flow cross section at the nozzle throat with similar swirling and nonswirling sonic lines. Since the mass flow rate through nozzle is primarily a function of throat density and axial Mach number, the reduction in the latter with swirl explains the observed reduction in mass flow at matched reservoir pressure. Greater pressures, on the other hand, result in higher throat densities, which compensates for the reduced axial Mach number, and the mass flow rate can be kept constant at its nonswirling value. It was also found that the distribution of subsonic Mach number (and not any of its components) in a swirling flow is solely dependent on cross-sectional area, similar to nonswirling flows; i.e., nonswirling and swirling flows have the same subsonic Mach number profile. In terms of thrust and specific impulse, the application of swirl at matched nozzle reservoir pressure results in the expected reductions in discharge coefficient, thrust, and specific impulse. At matched mass flow, however, the application of swirl results in the enhancement of both thrust and specific impulse. This is attributed to the considerable degree of underexpansion associated with the swirling flow as a result of the higher nozzle reservoir pressure with swirl.

Nomenclature

A	=	cross-sectional area
D	=	nozzle-exit diameter (11 mm)
F	=	nozzle thrust
I_{sp}	=	nozzle specific impulse
M	=	Mach number
$\dot{m}$	=	mass flow rate
p	=	pressure
R	=	specific gas constant
r	=	radial coordinate
S	=	swirl number
T	=	temperature
v	=	velocity
z	=	axial coordinate
γ	=	ratio of specific heats
ρ	=	density

Subscripts

a	=	axial
t	=	tangential

I. Introduction

HYPERSONIC vehicles, powered by scramjet engines, are pivotal for the future of high-speed flight. The critical science issues in hypersonic research under in-flight conditions have not been fully understood yet. These issues include mixing in supersonic airbreathing engines. It is desired to maintain supersonic flow through the combustor of a scramjet engine, to reduce the losses in total pressure and temperature inherent in decelerating the flow to subsonic speeds. Extensive investigations are still needed to achieve better understanding of the complicated flow dynamics and chemistry involved with the final goal of improved efficiency and performance. Successful operation of any airbreathing system depends primarily on efficient mixing of the injected fuel with airflow. The efficiency of an injection system is defined by the achievable degree of fuel/air mixing. Supersonic flows are compressible and resistant to fuel penetration and mixing. Therefore, the equivalence ratio of scramjet-engine operation has to be fuel-rich over a considerable part of the vehicle flight, to ensure that a flame is present to provide positive thrust. Any progress made on improving the engine efficiency must, therefore, be closely followed toward achieving efficient mixing between fuel and air. Scramjet flows have residence times of the order of only few milliseconds. In this short residence time, one must account for the mixing, ignition delay, and combustion time scales.

Swirl is one of the solutions of interest to the problem of poor supersonic mixing. The mixedness of a supersonic fuel jet injected into the supersonic airflow of a scramjet engine can be improved by imparting swirl to the fuel jet. This is achieved practically by tangential injection of fuel into its plenum and allowing the flow to accelerate through a nozzle. In other words, a subsonic swirling flow accelerates to supersonic speeds in a choked nozzle. Swirling compressible flows occur also in a variety of other practical applications, including turbofans and turbojet engines, integral rocket/ramjets, and fluidic vortex valves. In the first case, the tangential velocity component is induced by the motion of turbine blades. For ramjets, experimental studies have demonstrated that the swirl generated by fixed vanes located in the dump combustor inlet can lead to significantly improved combustor performance [1]. Clearly, the generated swirl in each of those propulsion systems will persist at some level to the inlet of exhaust nozzle. The behavior of a transonic swirling flow is thus of practical importance, which motivated this current study to examine the effect of axisymmetric vorticity on nozzle flowfield, so that design parameters such as thrust and mass flow rate can be accurately determined.

Subsonic swirling flows have been examined extensively in the literature, but little fundamental nature is known of the supersonic flows. Quasi-one-dimensional theories apply very well as a first

Received 2 November 2009; revision received 5 April 2010; accepted for publication 6 April 2010.

*Graduate Student, Department of Mechanical Engineering, 2181 Glenn Martin Hall. Student Member AIAA.

†Distinguished University Professor, Department of Mechanical Engineering, 2181 Glenn Martin Hall. Fellow AIAA.

approximation in nonswirling supersonic flowfields, but previous attempts to extend those theories to swirling supersonic flows have all failed, due to the intrinsic three-dimensionality of such flows. The most fundamental problem is the identification of choking criteria. One-dimensional theories without swirl prove that the throat Mach number is unity, implying that the mass flux through the throat of a fixed-geometry nozzle is maximum and that the throat velocity is equal to the speed of sound. The first criterion of maximum mass flux can be carried over to the swirling flowfield with known stagnation conditions. It is still not clear, however, how the second criterion applies to choked swirling flows. Because of the nonuniform throat velocity distribution, it is difficult in the absence of computational fluid dynamics (CFD) numerical simulations to predict which velocity or velocity component is equal to the local speed of sound. The maximum-mass-flux criterion has been used by several investigators. It was originally introduced by Mager [2] in his theoretical study of choked free-vortex flows with the ratio of specific heats $\gamma = 1.40$. His results were extended by Swithenbank and Sotter [3] to the case of $\gamma = 1.25$, and Glick and Kilgore [4] presented results for γ in the range 1.10–1.28.

The analysis of the free-vortex case is simplified by the fact that it is a potential flow, whereas the forced-vortex flow is truly rotational. This may be the reason why there have been several unsuccessful attempts to derive analytical expressions for the output characteristics of nozzles with choked flows. Bastress [5] tried to use the sonic velocity criterion by incorrectly assuming that the velocity magnitude was constant across each section and equal to the critical velocity at the throat. In addition, he assumed forced-vortex flow at all stations. Manda [6] used the constant-stagnation-enthalpy assumption to derive an equation for the axial velocity. Forced-vortex flow was again assumed at all stations, but this time the equality of velocity magnitude and critical velocity at throat were assumed to be satisfied only on the nozzle axis at the throat. King [7] proposed another solution in which he pointed out that the assumption of forced-vortex flow cannot hold everywhere, as it renders the problem overspecified. Manda [8], however, showed that King's solution violated the radial momentum equation. Finally, all the preceding papers were summarized and discussed by Hsu [9], who concluded that the basic reason behind the controversy lies in the fact that the one-dimensional approximation could not be applied to swirling flows.

Lewellen et al. [10] developed an approximation that can be used to determine how swirl affects the choking constraint on flow through the throat of a nozzle. It was found that the mass flow rate through a choked nozzle can be sharply reduced by introducing a tangential component of velocity into the flow. Moreover, the choking constraint imposes a limit on the maximum tangential Mach number that can be achieved in a vortex tube, even when an infinite pressure ratio is available. The theoretical choking constraint was used to speculate on the limiting tangential Mach number. It was concluded that this limiting value is 1.2, which is consistent with the experimental observations of Roschke and Pivirotto [11], who reported a value of 1.05. Toomre [12] achieved a value of 1.03, independent of mass flow rate, and Pinchak and Poplawski [13] reported a value of 1.18.

In a recent study, Gany et al. [14] analyzed inviscid (isentropic) choked swirling flows by introducing a theoretical model that can accommodate a general swirl type. The model was tested on three specific swirl types: namely, solid-body rotation, free-vortex flow, and an exponential dependence of the tangential velocity on the radial location. Their analysis was based on the following assumptions:

1) The radial velocity and its derivatives can be neglected.

2) The tangential velocity profile at any cross section can be described by the product of its value at the wall (varies from one cross section to the next) and a general nondimensional function of the radial location only.

The first assumption was justified by the findings of Lewellen et al. [10] and Batson and Sforzini [15]. The second assumption, on the other hand, was based on the fact that the conservation of angular momentum along a streamline implies similarity of the tangential velocity profile at each cross section. The authors forced a choking criterion that is based entirely on the axial-velocity component. This criterion "may yield good approximations in cases involving low swirl intensities," according to the authors, since the flow approaches the known nonswirling isentropic solution. However, that choking criterion is expected to fail at high degrees of swirl. Some of the key findings of this study include the following:

1) The axial-velocity profile changes, and its shape depends on the tangential velocity profile.

2) The axial Mach number at the throat exceeds unity within part of the cross section, in contrast to what is known for nonswirling flows.

3) The tangential Mach number at the nozzle throat wall increases as a result of increasing the swirl number for all examined swirl types. No prediction of any limiting value on the tangential Mach number was made.

4) The mass flow rate through the nozzle decreases as the swirl number increases, for the same stagnation pressure.

The lack of comprehensive understanding of supersonic swirling flows has also led to a controversy in terms of nozzle thrust and specific impulse. While some studies showed that the discharge coefficient, thrust, and specific impulse decrease with swirl, others reported that thrust can be increased with swirl. It is thus of fundamental as well as practical importance to determine how the nozzle propulsive characteristics are affected by the application of swirl.

Batson and Sforzini [15] studied the structure of swirling flow through a convergent nozzle with emphasis on the effect of swirl on flowfield, thrust, and mass flow produced by nozzled devices, such as jet engines and spin-stabilized rockets. It was reported that the axial-velocity component increases, whereas the tangential component decreases, as the flow passes through nozzle throat. In another study, which has application in ramjets and turbojets, Kornblum et al. [16] presented an analytical performance prediction methodology for annular propulsive nozzles, with swirl introduced in the combustor upstream of the nozzle. This methodology was applied to a specific nozzle design for a free-vortex swirl distribution. The results showed that the discharge coefficient, thrust, and specific impulse decrease as the amount of swirl is increased. Application of the prediction methodology to swirl distributions other than free vortex was recommended for future work. Hoffman et al. [17] followed this recommendation by applying this methodology to examine the effects of swirler design on nozzle performance. Four types of swirlers were investigated: namely, free-vortex, constant-angle, forced-vortex, and Rankine-vortex swirlers. The computed results indicated again that swirl decreases the discharge coefficient, thrust, and vacuum specific impulse. The decrease in discharge coefficient correlates with the mass-averaged swirl for all four types of swirlers. The decrease in vacuum specific impulse, on the other hand, is a function of swirler design. Forced-vortex swirlers induce the least reduction in specific impulse, whereas free-vortex swirlers induce the greatest reduction.

Based on the aforementioned review it can be seen that the choking criteria of a swirling flow through a supersonic nozzle are not fully understood yet. All previous analytical attempts (either to extend quasi-1-D theory to swirling supersonic flows or to introduce theoretical models that can accommodate a general swirl type) have failed to determine the correct choking criteria that represent the flow behavior accurately at any swirl intensity. It is not yet known which velocity component is choked (if any) and what the limiting tangential Mach number should be. A nearly unanimous agreement might exist in the literature that swirl induces reduction in the nozzle discharge coefficient, but no explanation ties this finding to a rigorous choking criterion. It is also not fully understood yet how swirl affects nozzle thrust and specific impulse. Therefore, further substantiation is needed in this regard.

The present work aims at resolving the aforementioned controversial issues by providing a numerical/experimental investigation of the choking criteria, thrust, and specific impulse of swirling underexpanded airflow through a choked convergent nozzle. Answers are provided for the following questions: What are the choking criteria? Is the throat velocity (or any of its components) equal to the local speed of sound in a swirling flowfield? If yes, does this apply in part of or all over the flow cross section, and how does

swirl affect the shape of the sonic line? How does swirl affect the subsonic Mach number, pressure, and temperature inside the nozzle and their transonic values across the throat? How does swirl affect the nozzle thrust and specific impulse?

As the analysis to be presented here will show, the answers to these questions are as follows: The throat velocity itself (and not any of its components) is choked in a swirling flowfield. Therefore, the limiting tangential Mach number is unity, and the application of swirl always results in a reduction in the axial Mach number component. The velocity is choked all over the flow cross section at the nozzle throat with similar swirling and nonswirling sonic lines. Since the mass flow rate through nozzle is primarily a function of throat density and axial Mach number, the reduction in the latter with swirl explains the observed reduction in mass flow at matched reservoir pressure. Greater pressures, on the other hand, result in higher throat densities, which compensates for the reduced axial Mach number, and the mass flow rate can be kept constant at its nonswirling value. The distribution of subsonic Mach number (and not any of its components) in a swirling flow is solely dependent on cross-sectional area, similar to nonswirling flows; i.e., nonswirling and swirling flows have the same subsonic Mach number profile. In terms of thrust and specific impulse, the application of swirl at matched nozzle reservoir pressure results in reductions in both thrust and specific impulse. At matched mass flow, however, the application of swirl results in the enhancement of both thrust and specific impulse. This is attributed to the considerable degree of underexpansion associated with the swirling flow as a result of the higher nozzle reservoir pressure with swirl.

II. Experimental Setup

The experimental investigation of this present work has been performed on the University of Maryland supersonic facility. The supersonic-nozzle assembly used is shown schematically in Fig. 1. This nozzle design was inspired by the work of Yu et al. [18], in which a similar design was used successfully to generate swirling underexpanded supersonic jets and examine the mode-switching phenomena of their screech-tone noise. A convergent nozzle of inlet-to-exit area ratio of 25 is used here to generate the examined underexpanded supersonic airflow. Reservoir pressures of up to about 9 atm (abs) are available, yielding near-field Mach numbers of up to 2.2 under nonswirling conditions. The reservoir pressure was measured using a Setra pressure transducer with a range of 0–500 psig and an accuracy of $\pm 0.13\%$ full scale. The nozzle has swirling capabilities, wherein the axial-tangential-entry technique with four tangential inlets is used to accurately control the degree of swirl imparted to airflow. This technique has been proven in previous research to be an efficient method for generating supersonic swirling jets [19–21]. Omega thermal flow meters/controllers are used to meter the flow rates of axial and tangential air components with an accuracy of $\pm 1.5\%$ full scale.

The nozzle was machined out of a single aluminum rod. Aluminum was preferred to stainless steel because the former has higher thermal conductivity, which prevents overheating of nozzle walls during combustion experiments. The higher conductivity allows radiated heat to be dissipated effectively through the thick nozzle walls. The dissipated heat is removed by forced convection of the entrained ambient cold air through the large surface area of nozzle external walls. The thickness of the nozzle lip was optimized to allow for significant entrainment of ambient air while having adequate rigidity for machining the exit section to the desired surface finish and dimensional tolerance.

Nozzle thrust was measured experimentally to assess the effect of swirl and provide validation for the numerical results. To measure the thrust, the nozzle assembly was connected to an Omega compression load cell (transducer) of 200 N capacity and $\pm 0.5\%$ full-scale accuracy.

III. Numerical Simulation Type and Assumptions

The commercial CFD-FASTRAN 2008 hybrid LES/RANS (large eddy simulation and Reynolds-averaged Navier–Stokes) code,

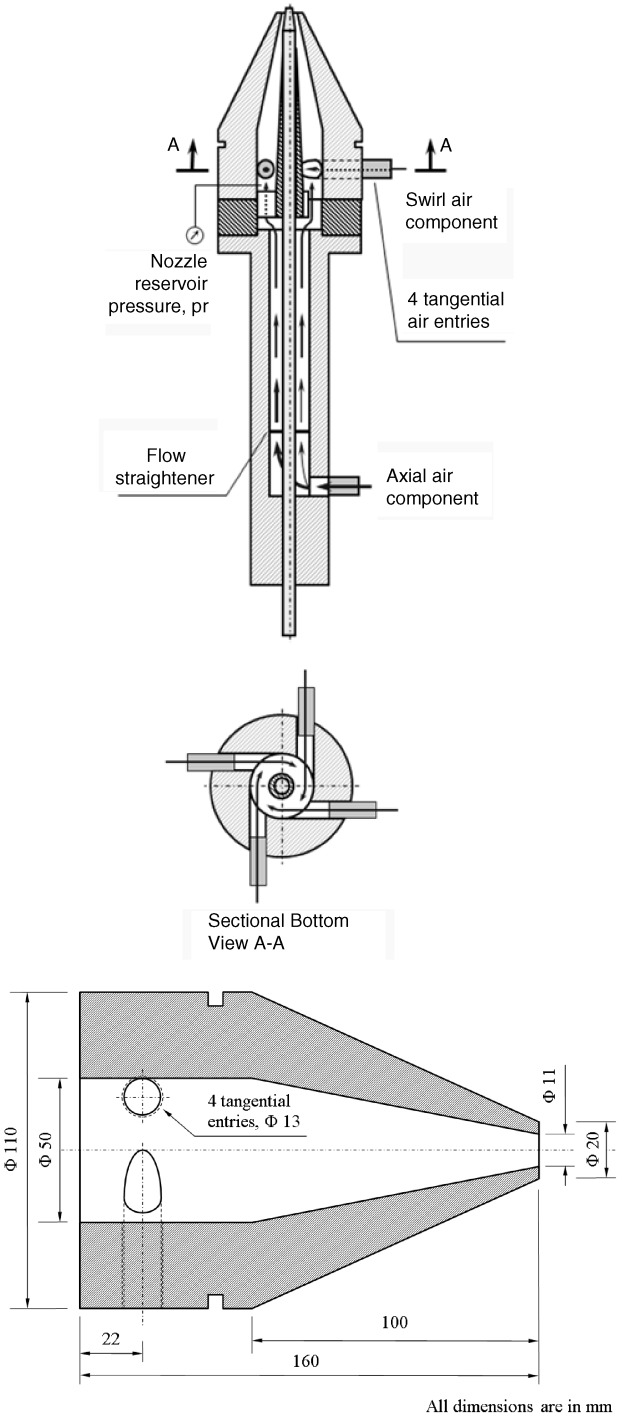

Fig. 1 Schematic of supersonic-nozzle assembly (top) and details of nozzle design (bottom).

provided by ESI-Group (formerly CFD Research Corporation), was used for all the simulations conducted in this study. To the authors' knowledge, the FASTRAN code has not been used before for simulating swirling underexpanded jets. The code was used, however, with a finite rate chemistry model at the Aeronautical Development Agency (ADA), India, to capture the flow and thermochemistry profiles of highly underexpanded nonswirling jets.[‡] The flow structure, barrel shocks, Mach disks, and shock diamond pattern were captured well. The code was also used at ADA to simulate higher-altitude effects on underexpanded jets at various conditions of altitude and flight Mach number. In another study

[‡]Data available online at http://www.esi-group.com/products/Fluid-Dynamics/cfd-fastran [retrieved 30 April 2010].

performed by the U.S. Air Force Research Laboratory, the FASTRAN code was used in conjunction with the CFD-ACE+ code (also provided by ESI-Group) to develop an integrated hierarchical design tool for simulation of unsteady flows and prototyping of flow control strategies in supersonic combustors [22]. An environment was developed that contains a number of control strategy implementations ranging from model-based indirect flow control to model-free direct control. The latter was applied successfully to control isolator unstart in a hypersonic combustor. The FASTRAN code was also used at the Center for Hypersonics, University of Queensland, Australia, to model shock-wave/boundary-layer interactions in hypersonic flows [23]. FASTRAN was used to replicate the conditions and geometry of a previously-tested experimental model and to predict the flow through another model designed to produce boundary-layer separation. It was concluded that the code was successful in characterizing the flow correctly for the existing experimental model. It should be noted here that the aforementioned review intends to cite some examples for relevant research performed by other institutions using the CFD-FASTRAN code. These examples are by no means limiting. The reader is encouraged to consult the literature for a more comprehensive review.

Since the nozzle examined here discharges a free supersonic flow into atmospheric backpressure, special emphasis was placed on the choice of boundary conditions that represent the flow surroundings. The entire nozzle assembly was surrounded by a cylindrical enclosure of 40D diameter and 70D length, where D is the nozzle-exit diameter (11 mm): a good representation of jet size (see Fig. 2). The 40D enclosure diameter ensures that the side boundaries are far enough from the jet, to eliminate any interference of both and to maintain constant near-stagnation atmospheric properties at the boundaries. Consequently, the bottom and side enclosure surfaces were assigned the fixed-pressure boundary condition, which matches the constant actual atmospheric ambient pressure. The top side of the enclosure, on the other hand, is an extrapolated outlet located 55D away from the nozzle exit ($\sim$78% of the 70D enclosure length). This guarantees that the flow leaves the simulated geometry shock-wave-free, since it was observed experimentally that complete transition to subsonic speeds occurs about 30D downstream of the nozzle exit.

Axisymmetry was enforced: i.e., only one quadrant of the geometry depicted in Fig. 2 was simulated. Special emphasis was placed on the level of cell skewness. The simulated geometry was subdivided into individual volumes, each meshed separately, to keep the skewness level of the most skewed cell below 0.5 (see Fig. 3a). A variable-size grid was generated with tetrahedral cells and a grid spacing ranging from 0.01 to 2.0 mm (see Fig. 3b). Grid spacing is defined here as the longest edge of the cell. Tighter meshing was implemented near and at the critical geometry locations: e.g., the exits of the nozzle and fuel-injection system. Mesh dependence was carefully examined through testing multiple levels of mesh tightness (see Fig. 3c). A total of 7,166,860 nodes per quadrant yielded the desired accuracy. Higher tightness levels did not result in significant accuracy enhancement and were thus not considered, to optimize the computational time.

Four subgrid RANS turbulence models from the FASTRAN library were tested for their capabilities to accurately predict a free swirling supersonic jet: namely, the k-ε, k-ω, Spalart–Allmaras, and Baldwin–Lomax [24] models. The parameters of each model were optimized to yield the least rms error, when compared with experimental data within the near-field supersonic flowfield up to 5D downstream of the nozzle exit. Figure 4a compares the obtained centerline static-pressure trace of each model to the corresponding experimental data. It can be clearly seen that the Baldwin–Lomax model offers the best agreement with experimental data among the available models within the FASTRAN code. Although several modifications of the Baldwin–Lomax model have been published, in attempt to enhance its prediction capabilities, it should be noted here that FASTRAN is not an open-source code, and none of those modifications is available. Nevertheless, the obtained degree of accuracy with the basic Baldwin–Lomax model was considered acceptable for the scope of this study.

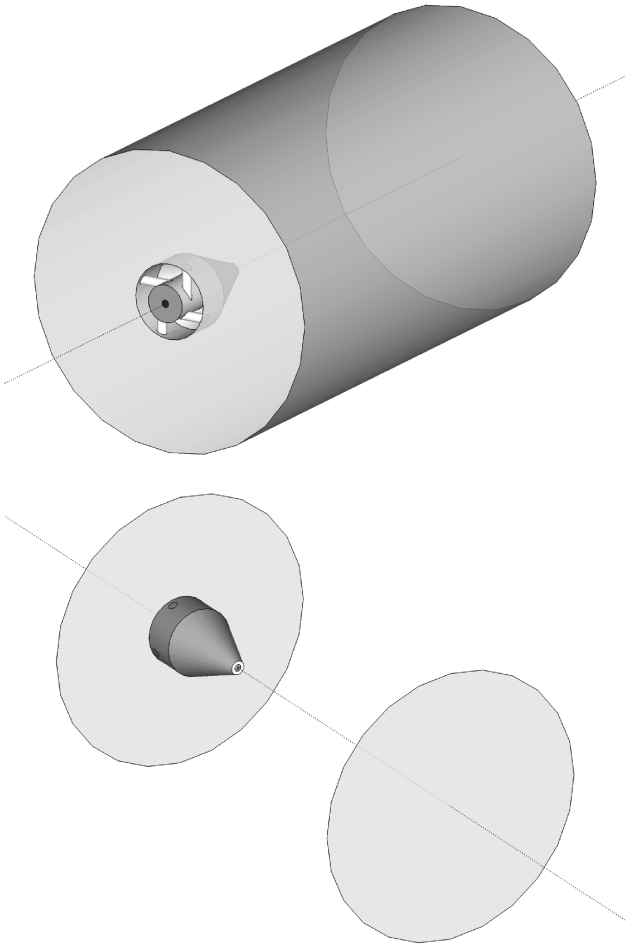

a)

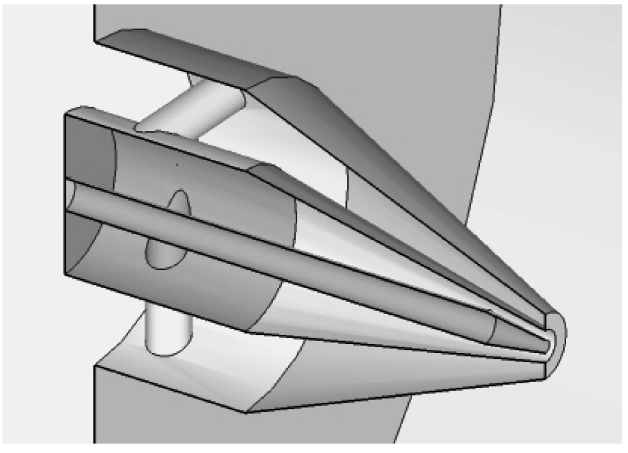

b)

Fig. 2 Illustrations of a) three-dimensional schematic of the numerically simulated geometry and b) zoom-in cutaway highlighting the nozzle details.

Calculation of the viscosity and conductivity was based on the kinetic theory of gases. A turbulent Schmidt number of 0.9 was used, and the mass diffusivity was calculated based on Fick's law with a Schmidt number of 0.5. A turbulent Prandtl number of 0.9 was used for calculating the turbulent conductivity. Similar to the experimental conditions, the total temperature at air inlets was kept fixed at 300 K, while the total pressure was kept at 7.91 bar without swirl and 8.82 bar with swirl. The 8.82 bar value was carefully chosen to ensure a common airflow rate of 175 g/s. The need for higher nozzle reservoir pressure with swirl is explained in detail in the Results and

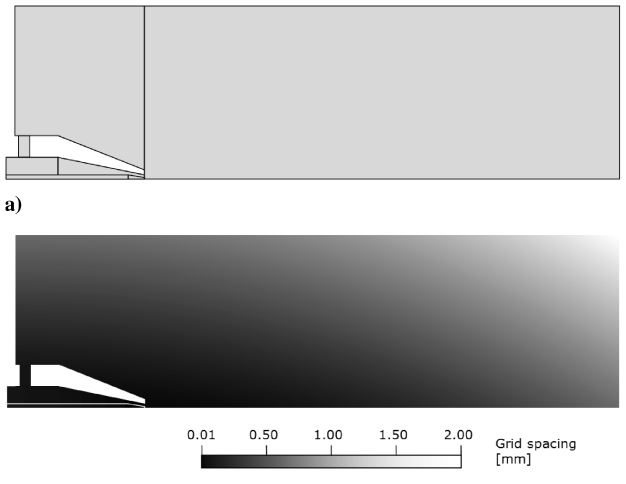

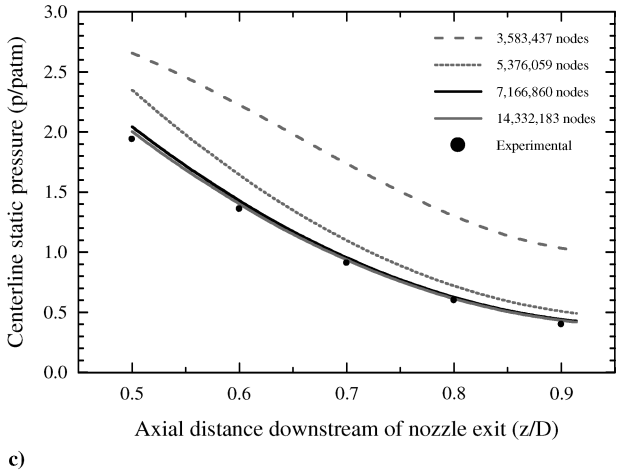

Fig. 3 Illustrations of a) individual subvolumes of the simulated geometry, b) grid spacing within a center plane, and c) mesh dependence and validation of numerical code (case 2).

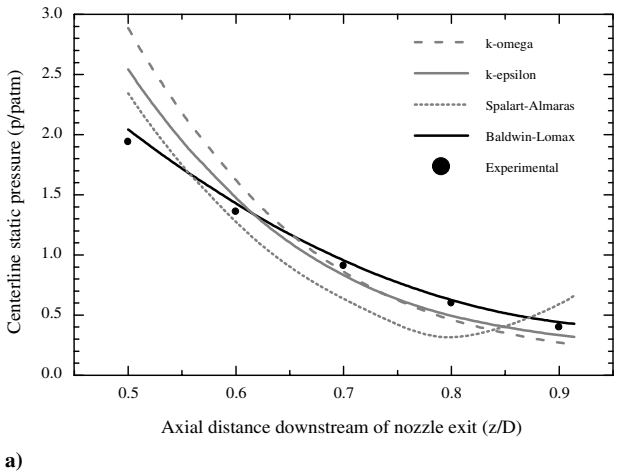

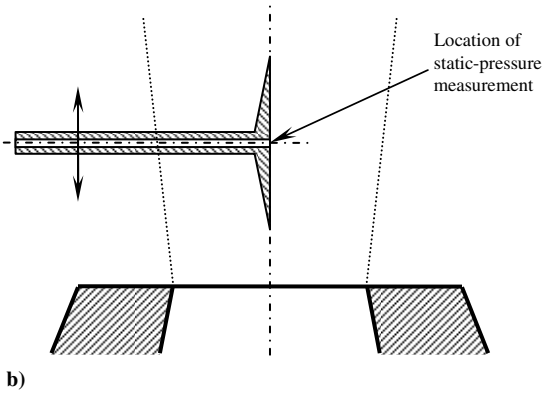

Fig. 4 Formulation and validation of numerical problem: a) choice of RANS turbulence model (case 2) and b) schematic presentation of how the centerline static pressure was measured experimentally for the sake of code validation.

Discussion section. The total pressure and temperature at air inlets were preserved throughout the iteration process in each examined case, until convergence was attained. Owing to the relatively large cross-sectional areas of the air inlets, the entrance Mach number was only about 0.02, resulting in almost identical inlet stagnation and static conditions.

The nozzle walls were set to be isothermal at 280 K, based on multiple temperature measurements of the nozzle interior and exterior walls. This is attributed to the aforementioned fact that the nozzle is made of aluminum, which has a high thermal conductivity and thus allows the nozzle to act as a near-isothermal body. The walls of the fuel-injection system, on the other hand, were set to be adiabatic, because the injection system is immersed almost totally into the nozzle and conditioning chamber, which allows for negligible amounts of heat to be conducted axially upstream through the thin walls of fuel system. Moreover, it is made of stainless steel that has a lower thermal conductivity (relative to aluminum).

The initial conditions of simulation were set for all cases at 1 atm static pressure, 300 K static temperature, 9.7 m/s axial velocity, and zero radial and tangential velocities. Consequently, the simulation incorporated the transient behavior as the high-pressure air expands and "marches" from the geometry inlet to the exit. An initial Courant–Friedrichs–Lewy number [25] of 0.1 was chosen that increases to unity as convergence is approached. Time integration is implicit, where a point Jacobi scheme was used, and a backward Euler discretization was implemented. Each case included 20,000 iterations. Convergence to 10^{-6} residuals was usually attained after 18,500–19,500 iterations.

IV. Test Matrix

The effect of swirl is investigated here by forwarding the entire airflow to nozzle tangential entries. This allows for examining a single degree of swirl: namely, the maximum attainable one. Consequently, the swirling cases in this study have the same geometrical swirl number of 0.36. The total pressure and temperature of air were kept constant at 7.91 bar and 300 K, respectively, for the nonswirling case presented here, which resulted in a fixed airflow rate of 175 g/s. It was noted, however, that imparting swirl to airflow at the same nozzle reservoir pressure of 7.91 bar results in reduced mass flow rate through the nozzle. This observation agrees with the findings of previous studies [10,16,17], in which it was proven that imparting swirl to the airflow results in additional choking of the nozzle, i.e., a lower mass flow rate compared with the corresponding nonswirling conditions at the same reservoir pressure. A theoretical limit of no flow was even predicted at an infinitely large swirl number. Therefore, a higher reservoir pressure is necessary to maintain the same flow rate through the nozzle. For the nozzle geometry, degree of swirl, and inlet-flow conditions examined in this study, it was found that a value of 8.82 bar yields identical airflow rates of 175 g/s in the nonswirling and swirling cases. Table 1 lists the cases examined here.

Table 1 Test matrix

Case	Reservoir pressure, bar	Total temp. at air inlet, K	$\dot{m}$, kg/s	S_g
1	7.91	300	0.175	0
2	8.82	300	0.175	0.36
3	7.91	300	0.150	0.36

V. Results and Discussion

A. Validation of Numerical Code

Before presenting any of the numerical results, code validation is demonstrated here by comparing the numerical centerline static-pressure trace within the near-field supersonic flowfield of case 2 to corresponding experimental data (see Figs. 3c and 4a). The centerline static pressure was measured experimentally within the near-field supersonic flowfield by inserting a knife-edge circular disc vertically inside the flow (see Fig. 4b). The disc has an outer diameter of $0.9D$ with a 0.5 mm internal channel for transferring the static-pressure signal to a 100 psi pressure transducer of 0.15 psi (0.01 bar) full-scale accuracy. The knife edge of the circular disc serves for cutting through the supersonic flow with minimum disturbance on the flat side, which is aligned with the nozzle centerline. It can be seen from Figs. 3c and 4a that the numerical code generally overpredicts the static pressure. This trend was observed to persist over the region of interest, which is composed of the subsonic flow inside the nozzle and the near-field supersonic flow up to $5D$ downstream of the nozzle exit. A maximum error of 7% was observed, which shows good agreement and was considered acceptable for the scope of this study.

In light of the aforementioned code-validation comparison it can be concluded the Baldwin–Lomax turbulence model is capable of predicting free supersonic swirling flows with good accuracy. This negates the common generic belief that this model poorly predicts swirling flows, which might be true under subsonic conditions but not under supersonic conditions, based on the findings of this study. Had the modified versions of the Baldwin–Lomax model been available in the FASTRAN code library, better prediction accuracy might have been achieved. The reader is referred to previous studies conducted by the authors [26,27], in which the Baldwin–Lomax model was successfully implemented in simulating confined supersonic flows using the hybrid LES/RANS FASTRAN code. The work of Dann and Morgan [23] is one more example of how the Baldwin–Lomax model outperforms the k-ω model in predicting boundary-layer separation in a shock-wave/boundary-layer interaction problem.

Another means of code validation is demonstrated here by comparing the experimentally measured thrust values to the numerically computed values. As will be seen later in the discussion of nozzle thrust and specific impulse, the computed and experimental thrusts differ by only 0.6–3.2%, which shows good agreement and confirms the capability of the numerical code to quantify the subsonic and throat flows with good accuracy.

B. Nozzle Choking Criteria

1. *Transthroat Flowfield*

Figure 5 examines the transthroat flowfield by comparing the flow sections about nozzle throat ($z/D = -0.1$ and $+0.1$). The radial variations of axial and tangential Mach number components (M_a and M_t) are shown in Figs. 5a and 5b, respectively. A significant increase in transthroat axial momentum is observed, which incorporates both jet acceleration and expansion. Significant radial expansion occurs in the absence of the restricting walls of the nozzle and injection system. On the other hand, a reduction in the magnitude of transthroat M_t is observed, which agrees with the findings of Batson and Sforzini [15]. Careful inspection of Fig. 5b, however, reveals that radial expansion results in an increase in angular momentum, which is undermined by the decrease associated with the reduction in magnitude of M_t. It is interesting to note here that the average tangential Mach number within the radial range $0.3 < r/D < 0.5$ in Fig. 5b compares very well with the findings of Gany et al. [14] when extrapolated to the swirl number of 0.36 examined here.

A notable observation to be made from Fig. 5a is that the transthroat magnitudes of M_a are subsonic over the entire flow cross section in the swirling flowfield. This is distinctly different from the findings of Gany et al. [14] and from the known behavior of nonswirling flow, where M_a transitions to supersonic values through the throat. Figure 5c explains such unusual behavior under swirling conditions. Shown is the radiation variation of overall transthroat Mach number M within the swirling flowfield. The expected

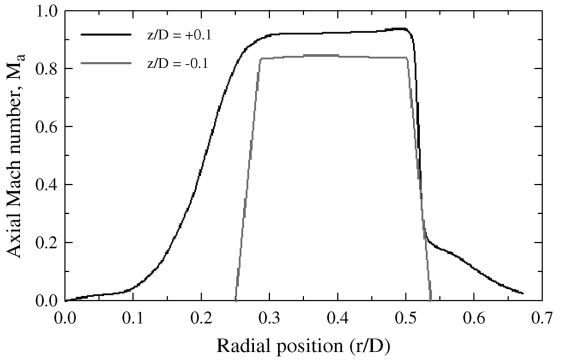

a)

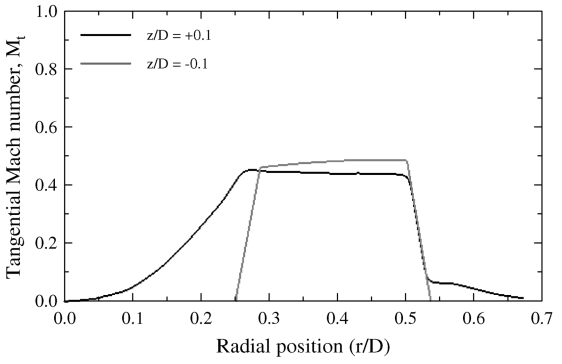

b)

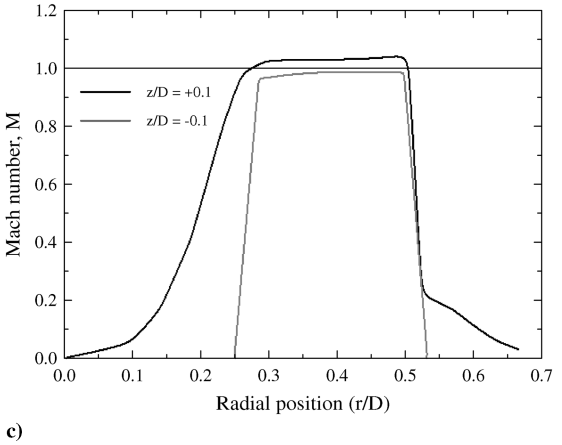

c)

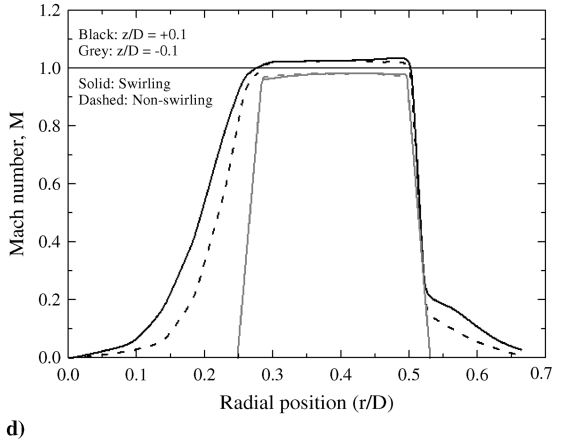

d)

Fig. 5 Plots of a) radial variation of transthroat axial Mach number component in case 2, b) radial variation of transthroat tangential Mach number component in case 2, c) radial variation of transthroat Mach number in case 2, and d) radial variation of transthroat Mach number in case 1 (nonswirling, dashed) and case 2 (swirling, solid).

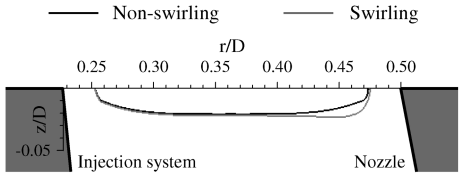

Fig. 6 Sonic lines in case 1 (nonswirling) and case 2 (swirling).

transition to supersonic propagation through nozzle throat is observed, which yields the main conclusion that both nonswirling and swirling flowfields behave similarly in terms of M, and not M_a. Such similarity exists on both the qualitative and quantitative scales, which is confirmed by Fig. 5d, in which the radial distributions of nonswirling and swirling transthroat Mach number are compared. The values of M within the jet ($0.26 < r/D < 0.47$) are very similar. Figure 6 further proves this fact by comparing the nonswirling and swirling sonic lines, which appear to be almost identical except at greater radii, at which the sonic line is reached earlier in the swirling flowfield. This agrees with the findings of Batson and Sforzini [15], in which it was reported that the flow velocity near the wall increases with swirl, due to Coriolis effects and area choking. The boundary layers are also identifiable in Fig. 6 beyond the radial range $0.26 < r/D < 0.47$.

2. Subsonic Flowfield Inside Nozzle

The remarkable similarity of transthroat nonswirling and swirling flows can even be traced back to the subsonic flowfield inside nozzle. Figure 7 shows the axial variations of cross-section-averaged subsonic Mach number. It is clearly noticeable how the nonswirling and swirling behaviors are almost identical, which strengthens the findings of Fig. 5d. The axial variations of nonswirling and swirling, total and static temperatures inside nozzle are shown in Fig. 8. Note that the throat static temperature varies within a range of about 10 deg only, which further proves the close similarity of nonswirling and swirling flowfields.

It should be noted at this point that the observed throat values of static temperature are considerably higher than what would be expected in isentropic flows. The isentropic value of sonic static temperature is 250 K in airflow of 300 K total temperature. This behavior can be explained by recalling that the nozzle examined here is made of aluminum. As mentioned earlier, the high thermal conductivity of aluminum allows the nozzle to be almost isothermal at a temperature of about 280 K. The relatively warmer entrained ambient air loses heat to the external nozzle walls, which is conducted to the inner walls and convected to the flow within. The fact that the airflow inside nozzle is gaining heat energy (i.e., not isentropic) is evident in Fig. 8, in which it can be clearly observed that the throat total temperature is considerably higher than its 300 K inlet value. If the flow were isentropic, it would have a constant total temperature throughout.

Further careful inspection of Fig. 8 reveals that the total temperature initially decreases below 300 K by about 5 deg in the

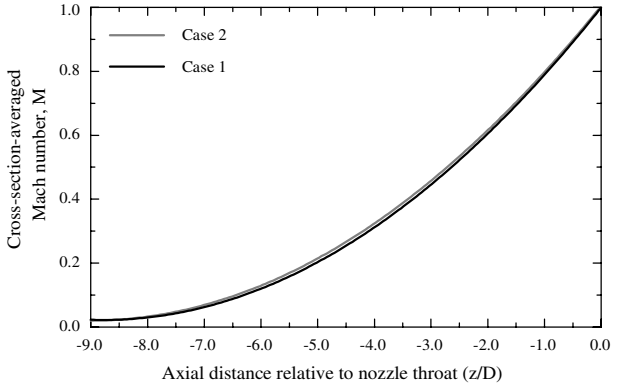

Fig. 7 Axial variations of cross-section-averaged subsonic Mach number in case 1 (nonswirling) and case 2 (swirling).

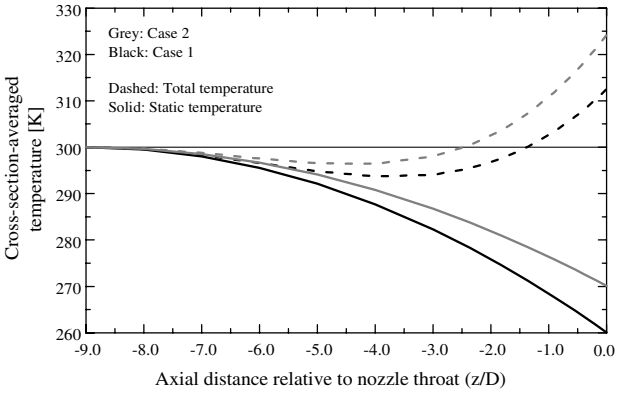

Fig. 8 Axial variations of cross-section-averaged total and static temperatures inside nozzle in cases 1 (nonswirling, black) and case 2 (swirling, gray).

upstream sections of nozzle before recovering and increasing beyond 300 K. This peculiar behavior can be explained by observing Fig. 9, in which a schematic representation of heat flow and static-temperature distribution is depicted. Note that the static temperature of nozzle flow decreases from 300 K at inlet to about 265 K at throat. Meanwhile, the stagnation temperature of ambient air is 300 K, and the temperature of nozzle walls was found experimentally to be almost constant at 280 K. It is expected to observe heat transfer from the ambient air to nozzle flow at the downstream sections. The heat flux is expected to increase as the flow approaches nozzle throat, because of the following:

1) The temperature difference between ambient air and nozzle flow increases.

2) The thickness of the nozzle wall decreases.

In other words, the potential for heat transfer increases, while the resistance decreases. This explains the greater rates of total temperature increase in Fig. 8 as the throat is approached. The peculiar observation, however, is that the 280 K nozzle walls are surrounded by warmer media on both sides at the upstream sections. This allows heat to be conducted axially downstream through the walls from both the ambient air and nozzle flow. The heat lost from the latter at the upstream sections explains the initial decrease in flow total temperature below 300 K, before recovery occurs at the downstream sections.

It might be argued here that these examined conditions do not compare directly to the fundamental isentropic quasi-1-D flow through nozzles, so how does the current analysis contribute to the understanding of the effect of swirl on such basic flow? The answer to this question is twofold. First, it was proven in the literature that one-dimensional approximation cannot be applied to swirling flows without either violating some conservation equations or enforcing assumptions that are too ideal for actual flows. Three-dimensional viscous numerical simulations, on the other hand, can now be implemented to study the behavior of such actual flows. Second,

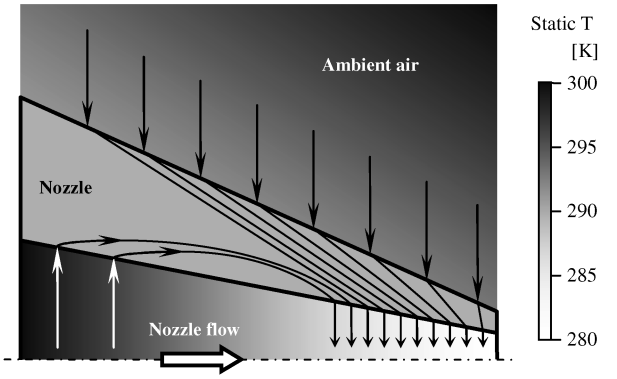

Fig. 9 Schematic representation of heat flow and static-temperature distribution.

nonisentropic nozzle flows with heat transfer through nozzle walls occur in a number of important practical propulsion applications, including turbofans and turbojet engines, spin-stabilized rockets, and integral rocket/ramjets. Heat transfer is essential for cooling the nozzle walls, especially near the throat section. The presented distributions of Mach number, pressure, and temperature might be specific to the examined geometry and flow conditions, which is also the case in many previous studies. Nevertheless, this study contributes significantly to the understanding of the effect of swirl on nozzle performance and flowfield, while highlighting the similarities and differences of nonswirling and swirling flows. No idealized assumptions are made, which would limit the applicability of the attained findings in engine/nozzle design or numerical-model development.

Having observed that the throat static temperature increases with the application of swirl, the question that arises here is how do viscous heating and heat transfer (from the relatively warmer 280 K nozzle walls) contribute individually to this temperature change. The answer to this question is discussed as follows. Consider case 3, which is a swirling case like case 2 but has the lower reservoir pressure of case 1. All three cases have the same inlet total temperature of 300 K. A side argument might be made here that the aforementioned Mach number similarity of nonswirling and swirling flows is attributed to the higher nozzle reservoir pressure with swirl, which leads to a common airflow rate. Figure 10, however, refutes this argument. Shown are the axial variations of Mach number inside nozzle for cases 1, 2, and 3. It is clearly evident that nonswirling and swirling flows are unconditionally similar in terms of Mach number, regardless of inlet conditions.

In terms of temperature, on the other hand, it is expected here that only the swirling cases 2 and 3 will behave identically. Both have the same swirl number, and the airflow is expected to experience the same total heat transfer through identical heat transfer rates and residence times. Figure 11a, however, shows that the resemblance is only qualitative. Depicted are the axial variations of total and static temperatures inside nozzle for cases 1, 2, and 3. It can be distinctly seen that case 3 is identical to neither case 1 nor case 2. If the airflow is treated as inviscid (through three more simulations, resulting in cases 1i, 2i, and 3i in Fig. 11b), however, the expected quantitative resemblance of the swirling cases is observed. This behavior is thus believed to be attributed to an implicit effect of total pressure on the viscous heating of the flow. It is known that pressure is a form of energy, i.e., the higher the flow pressure is, the greater is its energy potential. This extra energy can be transformed to other forms within the flow: e.g., viscous heating. If case 3 is compared with case 2 from this point of view, it can be deduced that the latter simply has more energy, some of which is dissipated in the form of viscous heating. Note that 175 g/s of air are forced through the nozzle in case 2, as compared with 150 g/s in case 3. In the absence of viscous heating, however, cases 2i and 3i show almost identical temperature profiles, which means that both cases have to experience almost identical heat

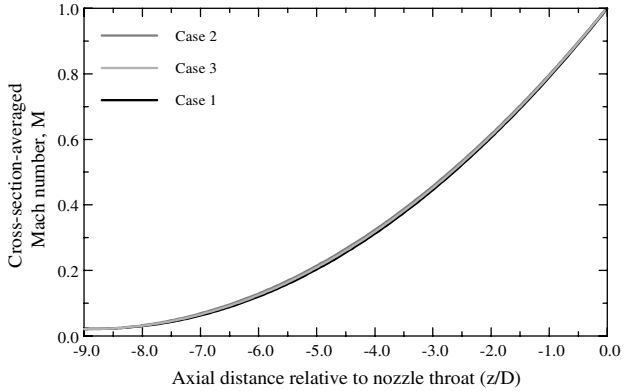

Fig. 10 Axial variations of cross-section-averaged Mach number inside nozzle; case 1 (nonswirling, reservoir pressure of 7.91 bar), case 2, (swirling, reservoir pressure of 8.82 bar), and case 3 (swirling, reservoir pressure of 7.91 bar).

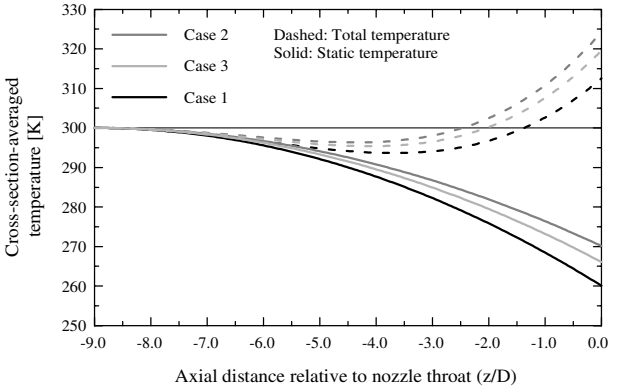

a) Isothermal nozzle walls, viscous flow

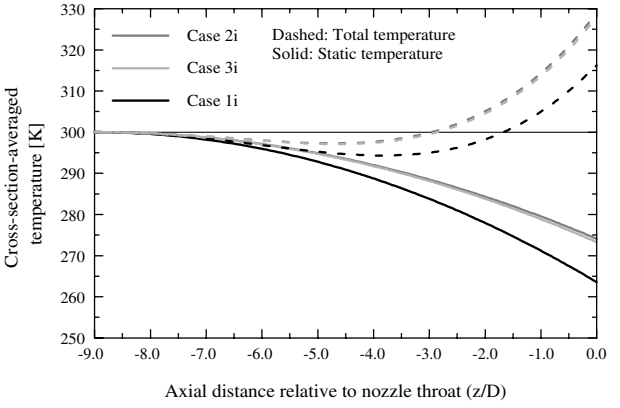

b) Isothermal nozzle walls, inviscid flow

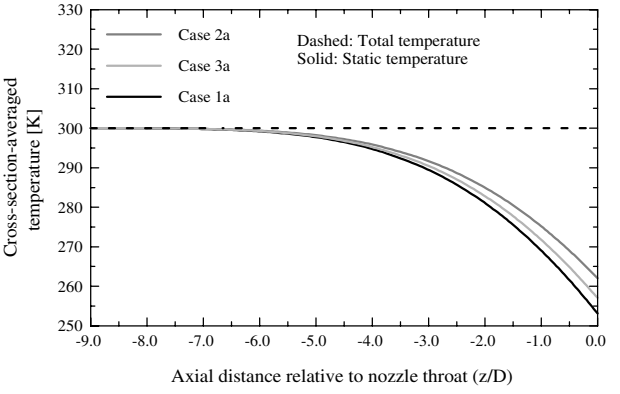

c) Adiabatic nozzle walls, viscous flow

Fig. 11 Axial variations of cross-section-averaged total and static temperatures inside nozzle; case 1 (nonswirling, reservoir pressure of 7.91 bar), case 2, (swirling, reservoir pressure of 8.82 bar), and case 3 (swirling, reservoir pressure of 7.91 bar).

transfers from the nozzle walls. Therefore, the conclusion to be made here is that increasing the reservoir pressure (and consequently the flow rate) from case 3 to case 2, while maintaining the same swirl number, results in viscous heating of the flow without any significant effect of wall heat transfer. This statement is confirmed by Fig. 11c, in which wall heat transfer is eliminated and the flow is treated as viscous in three additional simulations, resulting in the adiabatic cases 1a, 2a, and 3a. It can be observed that the transition from cases 3a to 2a results in a $\sim$6 deg increase in throat static temperature, which can only be attributed to viscous heating of the flow.

If cases 1 and 3 are to be compared now, one should note first that both start off with the same energy level (same inlet total temperature and pressure). Figure 11b reveals that the swirling flow of case 3i gains significantly more heat from the nozzle walls, while Fig. 11c shows that the application of swirl under adiabatic conditions results in some viscous heating of the flow. Both the effects of heat transfer

and viscous heating thus combine to yield the difference between the actual flows of cases 1 and 3 observed in Fig. 11a. It should be noted, however, that this combination is not a simple superposition of both effects, since wall heat transfer is significantly enhanced in the absence of flow viscosity and wall boundary layers, as observed from Figs. 11a and 11b.

Having analyzed the Mach number and total and static temperatures, the discussion proceeds to analyzing the effect of swirl on the total and static pressures. Figure 12 shows the subsonic axial variations of total and static pressures for cases 1, 2, and 3. The first important observation to be made is that increasing the reservoir pressure (and consequently the flow rate) from case 3 to case 2 results in significant loss of total pressure (in form of viscous heating), as evidenced from the comparison of the individual reductions in total pressure. This agrees with the aforementioned findings of Fig. 11. The second observation to be made is that only a small portion of pressure energy is consumed in additional viscous heating when case 1 is swirled at matched nozzle reservoir pressure to become case 3. This shows that wall heat transfer and flow viscous heating do not contribute equally to the observed difference in temperature between cases 1 and 3; the effect of wall heat transfer is more significant.

3. Swirl-Induced Choking

A fundamental question arises at this point: If the application of swirl at matched nozzle reservoir pressure (i.e., cases 1 and 3) results in minor changes in throat static pressure and temperature, then what causes the significant reduction in flow rate with swirl? Recall that the mass flow rate is the product of throat density, cross-sectional area, and axial-velocity component, i.e.,

$$\dot{m} = (\rho A v_a)_{\text{throat}} = \left(\frac{p}{RT} A M_a \sqrt{\gamma RT}\right)_{\text{throat}}$$

If the minor changes in throat static temperature are neglected, the above equation reduces to

$$\dot{m} \propto (pM_a)_{\text{throat}} \tag{1}$$

Recall from the analyses of Figs. 5a, 5d, and 10 that nonswirling and swirling flows are similar in terms of overall Mach number (M) and not axial Mach number component (M_a). At the throat, $M_a = M = 1$ in nonswirling flows, but $M_a < M = 1$ in the swirling flows. Therefore, the application of swirl results in a reduction in axial Mach number component. If no measures are taken toward increasing the nozzle reservoir pressure (cases 1 and 3), the throat static pressure remains almost unchanged (Fig. 12), and Eq. (1) dictates that the mass flow rate will decrease. The greater reservoir pressure of case 2, on the other hand, results in a higher throat static pressure, which compensates for the reduced axial Mach number component with swirl, and the mass flow rate can thus be kept constant at its nonswirling value. This explains the need for higher nozzle reservoir pressure with swirl to avoid reduction in mass flow rate.

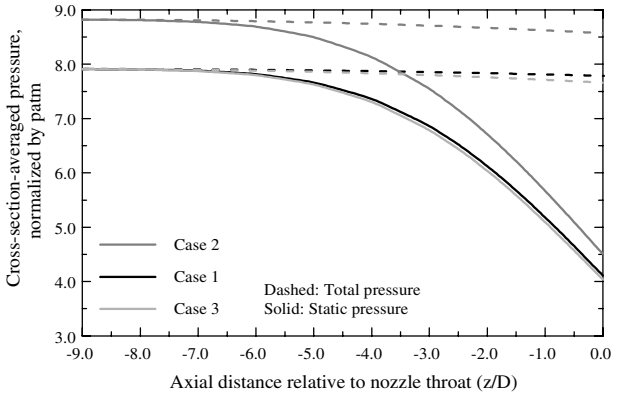

Fig. 12 Axial variations of cross-section-averaged total and static pressures inside nozzle; case 1 (nonswirling, reservoir pressure of 7.91 bar), case 2, (swirling, reservoir pressure of 8.82 bar), and case 3 (swirling, reservoir pressure of 7.91 bar).

The analysis of the nozzle flowfield is concluded here by a remark that pertains to the tangential component of Mach number M_t. It has been observed that the limiting Mach number in a swirling flowfield is the overall Mach number. It reaches its sonic value at the throat, independent of flow rate and inlet conditions, which means that all three components of Mach number are intrinsically subsonic. At extremely high degrees of swirl the value of tangential component approaches that of overall Mach number, which is believed to remain sonic at the throat. It should be noted here that this could not be examined experimentally in this study. No numerical simulations were conducted either in this regard, as they would not be considered a solid reference in the absence of experimental validation. Nevertheless, the current findings of this study support those of Toomre [12] and Roschke and Pivirotto [11], in which it was reported that the limiting tangential Mach number is almost unity. The findings of Lewellen et al. [10] and Pinchak and Poplawski [13], who reported values of 1.2 and 1.18, respectively, are, however, questioned here but not refuted.

C. Effect of Swirl on Thrust and Specific Impulse

In light of the analysis of the nozzle flowfield, the effect of swirl on nozzle thrust F and specific impulse I_{sp} can now be quantified. The former is calculated here as follows. From the integral form of momentum equation,

$$\int \rho \mathbf{v}(\mathbf{v} \bullet \hat{n})\, \mathrm{d}A = -\int p\hat{n}\, \mathrm{d}A + \mathbf{F}$$

If the entire nozzle assembly is taken as the control volume, the axial component of the above equation simplifies to

$$F = (pA)_{\text{throat}} + \dot{m} v_{a,\text{throat}} \tag{2}$$

Note that the axial component of airflow enters the nozzle assembly radially (see Fig. 1). Thus, the terms $(pA)_{\text{inlet}}$ and $(\dot{m}v_a)_{\text{inlet}}$ are excluded from the axial momentum equation. The same applies for the tangential entries as well. The specific impulse is defined as

$$I_{\text{sp}} = \frac{F}{\dot{m}g} \tag{3}$$

Applying Eqs. (2) and (3) to cases 1, 3, and 2, Table 2 can be obtained. Note that wall friction losses ($\int \tau_w\, \mathrm{d}A$) were not accounted for in the calculation of thrust, which explains why the numerically obtained values are higher than the experimentally measured values. Also note that the listed thrust values serve only for validation of numerical code, in which very good agreement can be observed. However, before any assessment can be made of the effect of swirl on nozzle thrust and specific impulse, the flows of cases 1, 2, and 3 have to be optimized by eliminating any degree of underexpansion. This can be achieved by considering a convergent–divergent (CD) nozzle that has the following characteristics:

1) The convergent section is identical to the nozzle examined here.

2) The exit-to-throat area ratio of the divergent section allows the flow to expand exactly to the atmospheric backpressure, which eliminates any degree of underexpansion and results in shock-free supersonic flow outside the CD nozzle within near-field region.

For the nonswirling flow of case 1, the necessary divergent section has an exit-to-throat area ratio of 1.685, which corresponds to an exit diameter of about $1.3D$. Since cases 2 and 3 cannot be fully optimized by the same divergent section, as they do not have the same throat static pressure of case 1, only the latter is optimized here, and any remaining degrees of over- or underexpansion in the swirling cases are tolerated.

This optimization procedure was conducted numerically in three more simulations of cases 1, 2, and 3, in which a CD nozzle was considered with an exit diameter of $1.3D$. The nozzle divergent section was designed using the method of characteristics. Table 3 lists the values of thrust and specific impulse after optimization.

Table 2 Degrees of underexpansion and the corresponding nonoptimized thrust and specific impulse values for cases 1–3

Case	$p_{\text{reservoir}}$, bar	p_{throat}, bar	$\dot{m}$, kg/s	F_{num}, N	F_{exp}, N	I_{sp}, s
1	7.91	4.11	0.175	87.6	87.0	50.7
3	7.91	4.04	0.150	79.5	77.0	52.3
2	8.82	4.51	0.175	91.6	89.0	51.8

Table 3 Values of thrust and specific impulse for cases 1–3 after flow optimization

Case	$p_{\text{reservoir}}$, bar	$\dot{m}$, kg/s	F, N	I_{sp}, s
1	7.91	0.175	99.2	57.8
3	7.91	0.150	84.0	57.1
2	8.82	0.175	106.1	61.8

Comparing cases 1 and 3 it can be clearly seen that the application of swirl at matched nozzle reservoir pressure results in reductions in the discharge coefficient, thrust, and specific impulse, which is in direct agreement with the findings of Kornblum et al. [16] and Hoffman et al. [17]. The effect of increasing nozzle reservoir pressure from case 3 to case 2 results in the expected thrust enhancement. The relative increase in mass flow is overtaken by a greater relative enhancement in thrust, and the specific impulse is thus increased as a result of increasing the nozzle reservoir pressure. If cases 1 and 2 are finally compared, it is clearly evident that the application of swirl at constant mass flux in a fixed-geometry nozzle results in the enhancement of thrust as well as specific impulse. This is mainly attributed to the considerable degree of underexpansion associated with the flow of case 2 at nozzle exit as a result of the higher nozzle reservoir pressure.

VI. Conclusions

The choking criteria, thrust, and specific impulse of swirling airflow through a choked nozzle have been investigated both numerically and experimentally in this study. The effects of swirl were examined at matched nozzle reservoir pressure as well as matched mass flow. The nozzle choking criteria with swirl were clearly described and used to explain the observed reduction in nozzle discharge coefficient with swirl. The following conclusions were made:

1) The throat velocity itself (and not any of its components) is choked in a swirling flowfield. Therefore, the limiting tangential Mach number is unity, and the application of swirl always results in a reduction in the axial Mach number component. The velocity is choked all over the flow cross section at the nozzle throat with similar swirling and nonswirling sonic lines, except at greater radii, at which the sonic line is reached earlier in the swirling flowfield.

2) Since the mass flow rate through nozzle is primarily a function of throat density and axial Mach number, the reduction in the latter with swirl explains the observed reduction in mass flow at matched reservoir pressure. Greater pressures, on the other hand, result in higher throat densities, which compensates for the reduced axial Mach number, and the mass flow rate can be kept constant at its nonswirling value.

3) The distribution of subsonic Mach number (and not any of its components) in a swirling flow is solely dependent on cross-sectional area, similar to nonswirling flows, i.e., nonswirling and swirling flows have the same subsonic Mach number profile.

4) The application of swirl at matched nozzle reservoir pressure results in the expected reductions in thrust and specific impulse. At matched mass flow, however, the application of swirl results in the enhancement of both thrust and specific impulse. This is attributed to the considerable degree of underexpansion associated with the swirling flow as a result of the higher nozzle reservoir pressure with swirl.

Acknowledgments

This work was supported by the Space Vehicle Technology Institute, jointly funded by NASA, U.S. Department of Defense, and U.S. Air Force within the NASA Constellation University Institutes Project (CUIP), with Claudia Meyer as the Project Manager. This support is gratefully acknowledged. The simulation packages CFD-GEOM, CFD-FASTRAN, and CFD-VIEW were provided by ESI-Group (formerly CFD Research Corporation). This support is gratefully acknowledged.

References

[1] Buckley, P. L., Craig, R. R., Davis, D. L., and Schwartzkopf, K. G., "The Design and Combustion Performance of Practical Swirlers for Integral Rocket/Ramjets," *AIAA Journal*, Vol. 21, No. 5, 1983, pp. 733–740. doi:10.2514/3.8141

[2] Mager, A., "Approximate Solution of Isentropic Swirling Flow through a Nozzle," *ARS Journal*, Vol. 31, No. 8, 1961, pp. 1140–1148.

[3] Swithenbank, J., and Sotter, G., "Vortex Generation in Solid Propellant Rockets," *AIAA Journal*, Vol. 2, No. 7, 1964, pp. 1297–1302. doi:10.2514/3.2535

[4] Glick, R. L., and Kilgore, M. S., "Effect of Specific-Heat Ratio on Mass Flow for Swirling Nozzle Flow," *Journal of Spacecraft and Rockets*, Vol. 4, No. 8, 1967, pp. 1098–1099. doi:10.2514/3.29027

[5] Bastress, E. K., "Interior Ballistics of Spinning Solid-Propellant Rockets," *Journal of Spacecraft and Rockets*, Vol. 2, No. 3, 1965, pp. 455–457. doi:10.2514/3.28204

[6] Manda, L. J., "Spin Effects on Rocket Nozzle Performance," *Journal of Spacecraft and Rockets*, Vol. 3, No. 11, 1966, pp. 1695–1696. doi:10.2514/3.28733

[7] King, M. K., "Comment on 'Spin Effects on Rocket Nozzle Performance'," *Journal of Spacecraft and Rockets*, Vol. 3, No. 12, 1966, pp. 1812–1813. doi:10.2514/3.28760

[8] Manda, L. J., "Reply by Author to M. K. King," *Journal of Spacecraft and Rockets*, Vol. 3, No. 12, 1966, p. 1813. doi:10.2514/3.61616

[9] Hsu, C., "Mass Blocking of Swirling Flow in Nozzles," *Journal of Spacecraft and Rockets*, Vol. 8, No. 12, 1971, pp. 1232–1234. doi:10.2514/3.30369

[10] Lewellen, W. S., Burns, W. J., and Strickland, H. J., "Transonic Swirling Flow," *AIAA Journal*, Vol. 7, No. 7, July 1969, pp. 1290–1297. doi:10.2514/3.5336

[11] Roschke, E. J., and Pivirotto, T. J., "Similarity in Confined Vortex Flows," Jet Propulsion Lab., TR 32-789, Pasadena, CA, 1965.

[12] Toomre, J., "Highly Swirling Flows Through a Convergent-Divergent Nozzle," M.Sc. Thesis, Massachusetts Inst. of Technology, Cambridge, MA, June 1963.

[13] Pinchak, A. C., and Poplawski, R., "On the Attainment of Extremely High Rotational Velocities in a Confined Vortex Flow," 2nd AIAA Annual Meeting, San Francisco, AIAA Paper 65-400, July 26–29, 1965.

[14] Gany, A., Mor, M., and Goldman, C., "Analysis and Characteristics of Choked Swirling Nozzle Flows," *AIAA Journal*, Vol. 43, No. 10, 2005, pp. 2177–2181. doi:10.2514/1.16887

[15] Batson, J. L., and Sforzini, R. H., "Swirling Flow through a Nozzle," *Journal of Spacecraft and Rockets*, Vol. 7, No. 2, 1970, pp. 159–163. doi:10.2514/3.29892

[16] Kornblum, B. T., Thompson, H. D., and Hoffman, J. D., "An Analytical Investigation of Swirl in Annular Propulsive Nozzles," *Journal of Propulsion and Power*, Vol. 2, No. 2, 1986, pp. 155–160. doi:10.2514/3.22860

[17] Hoffman, J. D., Thompson, H. D., and Marcum, D. L., "Analytical Study of Swirler Effects in Annular Propulsive Nozzles," *Journal of Propulsion and Power*, Vol. 3, No. 5, 1987, pp. 465–466. doi:10.2514/3.23011

[18] Yu, Y. K., Chen, R. H., and Chew, L., "Screech Tone Noise and Mode Switching in Supersonic Swirling Jets," *AIAA Journal*, Vol. 36, No. 11, 1998, pp. 1968–1974. doi:10.2514/2.323

[19] Gupta, A. K., Lilley, D. G., and Syred, N., *Swirl Flows*, Abacus Press, London, 1984.

[20] Cutler, A. D., Levey, B. S., and Kraus, D. K., "Near-Field Flow of

Supersonic Swirling Jets," *AIAA Journal*, Vol. 33, No. 5, 1995, pp. 876–881.
doi:10.2514/3.12362

[21] Linck, M., "Spray Flame and Exhaust Jet Characteristics of a Pressurized Swirl Combustor," Ph.D. Thesis, Univ. of Maryland, College Park, MD, May 2006.

[22] Pindera, M. Z., and Athavale, M. M., "Multi-Scale Software Tool for Controls Prototyping in Supersonic Combustors," U.S. Air Force Research Lab., Rept. AFRL-PR-WP-TR-2004-2119, Wright-Patterson AFB, OH, April 2004.

[23] Dann, A. G., and Morgan, R. G., "CFD Designed Experiments for Shock Wave/Boundary Layer Interactions in Hypersonic Ducted Flows," *16th Australian Fluid Mechanics Conference*, Gold Coast, Australia, Dec. 2007, pp. 1304–1308.

[24] Baldwin, B. S., and Lomax, H., "Thin Layer Approximation and Algebraic Model for Separated Turbulent Flows," 16th AIAA Aerospace Sciences Meeting, Huntsville, AL, AIAA Paper 78-257, Jan. 16–18, 1978.

[25] Courant, R., Friedrichs, K., and Lewy, H., "On the Partial Difference Equations of Mathematical Physics," *IBM Journal of Research and Development*, Vol. 11, Mar. 1967, pp. 215–234.
doi:10.1147/rd.112.0215

[26] Abdelhafez, A., and Gupta, A. K., "Numerical Investigation of Oblique Fuel Injection in a Supersonic Combustor," 46th AIAA Aerospace Sciences Meeting and Exhibit, Reno, NV, AIAA Paper 2008-0068, Jan. 2008.

[27] Abdelhafez, A., Gupta, A. K., Balar, R., and Yu, K. H., "Evaluation of Oblique and Traverse Fuel Injection in a Supersonic Combustor," 43rd AIAA/ASME/SAE/ASEE Joint Propulsion Conference & Exhibit, Cincinnati, OH, AIAA Paper 2007-5026, July 2007.

J. Oefelein
Associate Editor